Intrasubband scattering in highly excited semiconductor quantum wells with biaxial strain

Shunji Seki and Kiyoyuki Yokoyama
NTT Opto-Electronics Laboratories, 3-1 Morinosato Wakamiya, Atsugi, Kanagawa 243-01, Japan

Paul Sotirelis
Beckman Institute, University of Illinois at Urbana-Champaign, 405 North Mathews Avenue, Urbana, Illinois 61801
(Received 15 November 1993; revised manuscript received 4 March 1994)

Intrasubband scattering rates are calculated for electrons and holes at finite temperatures in highly excited semiconductor strained-layer quantum-well structures. Carrier-carrier and carrier-phonon interactions are taken into account on an equal basis within the fully dynamic random-phase approximation for multisubband structures. It will be shown that the strain-induced changes in the valence-band structure exert a significant influence on the scattering rates of the electrons as well as the holes. The screening of carrier-phonon interaction by the electron-hole plasma in the coupled electron-hole-phonon system is discussed and analyzed.

I. INTRODUCTION

The relaxation mechanism of charge carriers (electrons and holes) in highly excited semiconductors has attracted much interest since it exerts significant influence on the electronic and optical properties of semiconductor devices. Of particular interest are many-body processes, such as the screening of the Coulomb interaction potential, carrier-carrier scattering, optical dephasing, etc., in the electron-hole plasma generated in semiconductors. These processes in highly excited semiconductors have been studied extensively not only in bulk (i.e., three-dimensional) materials[1-4] but also in quantum-well (i.e., quasi-two-dimensional) structures.[5-9] Although a conventional quantum-well (QW) structure consists of a stack of *lattice-matched* semiconductor layers, recent progress in epitaxial growth techniques has made it possible to produce a *strained-layer* (SL) quantum-well structure in which a thermodynamically stable semiconductor thin film undergoes an internal elastic biaxial strain due to the lattice mismatch. With these SL QW structures, we have entered a new era not only in electronic but also in optoelectronic semiconductor devices.[10-13]

One of the successful applications of SL QW structure is the semiconductor laser, which was proposed by Yablonovitch and Kane[12] and Adams.[13] Biaxial strain applied to the QW can vary the degree of valence-band mixing, which makes it possible to realize the tailor-made valence-band structure with the desired in-plane effective mass by adjusting the amount of strain in either direction (either compressive or tensile).[14,15] This idea of *valence-band engineering* has led to a significant improvement in threshold currents and other device properties of semiconductor lasers as predicted.[12,13] The excitation and relaxation of charge carriers in the electron-hole plasma play a principal role in determining laser dynamics.[16] Therefore, it has become very important to clarify the influence of the strain-induced changes in the valence-band structure on the many-body processes in highly excited semiconductor SL QW structures that relate to device performance.

In general, charge carriers can relax through a variety of scattering processes, including carrier-carrier scattering, acoustic- or LO-phonon emission, etc. Since the relaxation process can be quite complex with these multiple processes simultaneously present, one has often taken the approach in which these processes are studied in an isolated manner.[4,5,17,18] However, it is known that, in polar semiconductors, the phonons and the electron gas are mutually interacting and affecting each other's properties.[2,3,6,7] In addition, it has been reported that the sum of the electron scattering rates obtained in an isolated manner becomes larger than the scattering rate obtained in the coupled electron-phonon system when the carrier density is very high.[19] Hence it is necessary to take into account carrier-carrier scattering and carrier-phonon scattering on an equal basis in the coupled electron-hole-phonon system.

There are two important frequencies in the coupled system: the LO-phonon frequency (ω_{LO}) and the plasma frequency (ω_{pl}) of the electron-hole plasma. Approximation schemes for the coupled system, corresponding to the limits $\omega_{LO} \ll \omega_{pl}$ or $\omega_{LO} \gg \omega_{pl}$, are given in many publications.[1-3] However, in the doped or excited semiconductors that we are interested in, the carrier density usually ranges from 10^{16} to 10^{19} cm^{-3}, which corresponds to the situation of $0.1\omega_{LO} \leq \omega_{pl} \leq 10\omega_{LO}$. Consequently, under these conditions the usual approximations are not applicable; we are interested in the intermediate-coupling regime. Furthermore, in III-V semiconductor compounds, the polar coupling (though weaker than in II-VI semiconductor compounds) is sufficiently strong such that its inclusion is necessary.[2,3,7]

In this paper, we calculate intrasubband scattering rates for electrons and holes in the lowest subband of $In_{1-x}Ga_xAs_yP_{1-y}$/InP SL QW structures at finite temperatures. (We refer to the subband nearest from the band edge of strained InGaAsP well as the *lowest sub-*

band throughout this paper.) Many-body processes are treated within the Born approximation including carrier-carrier interactions and carrier–LO-phonon interactions on an equal basis. We demonstrate here that the strain-induced changes in the valence-band structure exert a significant influence on the scattering processes for both charge carriers. We also discuss the mutual interactions between the phonons and the electron-hole plasma in highly excited semiconductor SL QW structures. In Sec. II the mathematical formulation for the calculation of the band structure and the intrasubband scattering rate is presented. The valence-band mixture and the strain effects are taken into account using the Luttinger-Kohn Hamiltonian. On the basis of these results, the average effective-mass approximation is introduced to extract the characteristic features of the strain-induced changes in the valence-band structure. The screening of the Coulomb and Fröhlich interactions are treated consistently in the fully dynamic random-phase approximation (RPA) including the carriers occupying multiple subbands. In Sec. III we briefly describe the characteristic features of the strain-induced changes in the valence-band structures on the basis of the $\mathbf{k}\cdot\mathbf{p}$ results. We then present a detailed discussion of the carrier scattering rates in the coupled electron-hole-phonon system. The effects of strain on the valence-band structures are directly correlated with the intrasubband scattering rates for both electrons and holes. The screening of the carrier-phonon interaction by the electron-hole plasma is also discussed in this section. A short summary of this work is given in Sec. IV. In the Appendix the $\mathbf{k}\cdot\mathbf{p}$ method used in the band-structure calculation for the SL QW is described in more detail.

II. MATHEMATICAL FORMULATION

A. Band structure

Band-structure calculations including the effects of strain are described in many publications.[15,20,21] Therefore, we just summarize the basic procedure. Valence-band structures are calculated on the basis of the multiband effective-mass theory and the deformation potential theory. In this formalism, the hole wave function is given by

$$|\Psi^h_{n,\mathbf{k}_\parallel}(\mathbf{r}_\parallel,z)\rangle=\sum_\nu e^{i\mathbf{k}_\parallel\cdot\mathbf{r}_\parallel}g^\nu_n(\mathbf{k}_\parallel,z)|\psi^h_\nu\rangle\ , \tag{1}$$

where $\mathbf{k}_\parallel$ is the in-plane wave vector, z is the coordinate perpendicular to the heterointerface, $\mathbf{r}_\parallel$ is the in-plane radial coordinate, n is a valence-subband index, and $|\psi^h_\nu\rangle$ is the Bloch function having spin symmetry ν at the center of the Brillouin zone. The envelope function $g^\nu_n(\mathbf{k}_\parallel,z)$ and subband energy $E^h_n(\mathbf{k}_\parallel)$ are obtained by solving the multiband effective-mass equation

$$\sum_{\nu'}[H^{\nu\nu'}_h+V_h(z)\delta_{\nu\nu'}]g^{\nu'}_n(\mathbf{k}_\parallel,z)=E^h_n(\mathbf{k}_\parallel)g^\nu_n(\mathbf{k}_\parallel,z)\ , \tag{2}$$

where $V_h(z)$ is the potential profile in the valence band of the well. In our calculations, we use a 4×4 Luttinger-Kohn Hamiltonian[22,23] for $H^{\nu\nu'}_h$, which includes a mixture of $|\frac{3}{2},\pm\frac{3}{2}\rangle$ and $|\frac{3}{2},\pm\frac{1}{2}\rangle$ states. Following the ideas of Broido and Sham,[24] we blockdiagonalize the Hamiltonian by a unitary transformation. For further analysis, we then apply the axial approximation, which has been shown to give a good description of valence-band structures.[25] Thus we can neglect the warping in the (k_x,k_y) plane. The electron envelope function $\phi^e_l(\mathbf{k}_\parallel,z)$ and subband energy $E^e_l(\mathbf{k}_\parallel)$ are then obtained by solving a simple scalar effective-mass equation

$$[H_e+V_e(z)]\phi^e_l(\mathbf{k}_\parallel,z)=E^e_l(\mathbf{k}_\parallel)\phi^e_l(\mathbf{k}_\parallel,z)\ , \tag{3}$$

where H_e is the conduction-band Hamiltonian, $V_e(z)$ is the potential profile in the conduction band, and l is a conduction subband index. Some more details concerning the Luttinger-Kohn and the conduction-band Hamiltonians including the effects of strain are described in the Appendix.

To extract the characteristic features of the strain-induced changes in the valence-band structures, we use the average effective-mass approximation[26,27] in which the coupled valence bands are approximated by a set of decoupled parabolic bands with averaged effective mass assigned according to the following procedure. For a given total hole density P, we first determine the quasi-Fermi level on the basis of the exact band structure using

$$P=\sum_n p_n$$
$$=\sum_n\int dE\,\rho^h_n(E)n_f(E^h_n(k_\parallel))\ , \tag{4}$$

where p_n is the subband carrier density of the nth valence subband, $\rho^h_n(E)$ is the nth subband's density of states calculated from the exact band structure, n_f is the Fermi distribution function, and $k_\parallel=|\mathbf{k}_\parallel|$. For each previously obtained quasi-Fermi level and subband carrier density, we then determine the averaged effective mass for each subband using

$$p_n=\int dE\frac{m^h_n}{\pi\hbar^2}n_f(E^{\rm av}_n(k_\parallel))\ . \tag{5}$$

Here m^h_n is the averaged effective mass assigned to the nth valence subband and $E^{\rm av}_n(k_\parallel)$ is the fitted parabolic band, which is given by

$$E^{\rm av}_n(k_\parallel)=\frac{\hbar k^2_\parallel}{2m^h_n}+E^h_n(k^{\rm min}_n)\ , \tag{6}$$

where $k^{\rm min}_n$ is the in-plane wave vector at which the nth subband reaches the band extrema. It should be noted that, for a given quasi-Fermi level, the exact band structure obtained by $\mathbf{k}\cdot\mathbf{p}$ theory and the approximated band structure obtained by the average effective-mass approximation yield exactly the same total carrier density and subband carrier densities. Within this approximation, the changes in the effective mass of each valence subband as well as in the actual valence-subband energy spacings (energy separation between the band extreme of subbands) are well described.[26]

B. Intrasubband scattering rate

The intraband (including both intrasubband and intersubband) scattering rate for electrons or holes $\Gamma^{\sigma}_{\mathbf{k}_1}$ ($\sigma=e,h$) is given by

$$\Gamma^{\sigma}_{\mathbf{k}_1}=\Gamma^{\sigma}_{\mathbf{k}_1\text{out}}+\Gamma^{\sigma}_{\mathbf{k}_1\text{in}} , \tag{7}$$

where $\Gamma^{\sigma}_{\mathbf{k}_1\text{out}}$ and $\Gamma^{\sigma}_{\mathbf{k}_1\text{in}}$ are the rates of scattering out of and into the momentum state $\mathbf{k}_1$, respectively. The general form of the intraband scattering-out rate for carrier σ is derived by using Fermi's golden rule and is expressed as[19]

$$\Gamma^{\sigma}_{\mathbf{k}_1\text{out}}=\frac{2\pi}{\hbar}\frac{2}{(2\pi)^2}\int d^2q[1-n_f^{\sigma}(E_i^{\sigma}(\mathbf{k}-\mathbf{q}))][n_b(\omega)+1] \times\frac{1}{2\pi}\text{Im}[-V^{\text{eff}}_{jiij}(\mathbf{q},\omega)] , \tag{8}$$

where $V^{\text{eff}}_{jiij}(\mathbf{q},\omega)$ denotes the screened Coulomb potential and i and j are the subband indices of the initial and final states, respectively. In this study, we focus our attention on the intrasubband scattering rate for carrier in the lowest subband in a quantum well. To properly treat the multisubband structures, we use an approximate analytic form of Eq. (8) that includes the effects of carriers occupying the higher subbands and the excitons between different subbands as described later in this section. Hence Eq. (8) is simplified such that the scattering-out rate for carrier σ in the lowest subband of the well is given by

$$\Gamma^{\sigma}_{\mathbf{k}_1\text{out}}=\frac{2\pi}{\hbar}\frac{2}{(2\pi)^2}\int d^2q[1-n_f^{\sigma}(E_1^{\sigma}(\mathbf{k}-\mathbf{q}))] \times[n_b(\omega)+1] \times\frac{v(q)f_{1111}(q)}{2\pi}\text{Im}\left[\frac{-1}{\epsilon_{1111}(q,\omega)}\right] . \tag{9}$$

We use the Fermi-Dirac statistical factor n_f since we focus our attention on the situation where a quasiequilibrium carrier distribution is realized, being most relevant to cw oscillated semiconductor lasers. The energy $\hbar\omega=E_1^{\sigma}(\mathbf{k})-E_1^{\sigma}(\mathbf{k}-\mathbf{q})$ is the energy loss of the scattered particle. The function n_b is the Bose statistical factor and $v(q)$ is the two-dimensional Fourier transform of the Coulomb interaction. $\Gamma^{\sigma}_{\mathbf{k}_1\text{in}}$ is obtained by replacing $1-n_f\leftrightarrow n_f$ and $n_b+1\leftrightarrow n_b$ in Eq. (9). The function f_{1111} represents a form factor involving the overlap of the electron (hole) wave functions $\phi_1(z)$ of the ground state and is given by

$$f_{1111}(q)=\int\int dz_1dz_2\phi_1^*(z_1)\phi_1(z_1) \times\exp(-q|z_1-z_2|)\phi_1(z_2)\phi_1^*(z_2) . \tag{10}$$

The function $\epsilon(q,\omega)$ in Eq. (9) is the complex RPA dielectric function. In this study, the RPA dielectric function assumes three different forms, each corresponding to one of the three cases studied; they are given by

$$\epsilon_{1111}(q,\omega)=\epsilon_{\infty}+\frac{(\epsilon_{\infty}-\epsilon_s)\omega_{\text{TO}}^2}{\omega^2-\omega_{\text{TO}}^2} , \tag{11a}$$

$$\epsilon_{\infty}-v(q)f_{1111}(q)\Pi^e_{11}(\mathbf{q},\omega)-v(q)f_{1111}(q)\Pi^h_{11}(\mathbf{q},\omega) , \tag{11b}$$

and

$$\epsilon_{\infty}+\frac{(\epsilon_{\infty}-\epsilon_s)\omega_{\text{TO}}^2}{\omega^2-\omega_{\text{TO}}^2} -v(q)f_{1111}(q)\Pi^e_{11}(\mathbf{q},\omega)-v(q)f_{1111}(q)\Pi^h_{11}(\mathbf{q},\omega) . \tag{11c}$$

The RPA dielectric functions, Eqs. (11a)–(11c), correspond to (i) the unscreened interaction with the phonons, (ii) the screened interaction with double-component electron-hole plasma neglecting the phonons, and (iii) the screened interaction with double-component electron-hole plasma coupled with the phonons, respectively. We assume dispersionless, bulk-type LO phonons. Here ω_{TO} is the TO-phonon frequency and is given by the Lyddane-Sachs-Teller relation

$$\omega_{\text{TO}}^2=\omega_{\text{LO}}^2\frac{\epsilon_{\infty}}{\epsilon_s} . \tag{12}$$

Within the RPA, the dynamical screening due to the carrier σ is determined by the Lindhard form and is given by

$$\Pi^{\sigma}_{11}(\mathbf{q},\omega)=2\sum_{l,\mathbf{k}}\frac{n_f^{\sigma}(E_l^{\sigma}(|\mathbf{k}+\mathbf{q}|))-n_f^{\sigma}(E_l^{\sigma}(|\mathbf{k}|))}{E_l^{\sigma}(|\mathbf{k}+\mathbf{q}|)-E_l^{\sigma}(|\mathbf{k}|)-\hbar\omega-i\varepsilon} . \tag{13}$$

To properly treat multisubband quantum-well structures using Eq. (9), the effects of the carriers occupying the higher subbands are taken into account by including the corresponding polarization terms in the dielectric function as shown in Eq. (13).

III. RESULTS AND DISCUSSION

A. Valence-band structure

We analyzed $In_{1-x}Ga_xAs_yP_{1-y}$ SL QW structures with a lattice-matched InGaAsP barrier ($E_g=1.31$ eV). We used quaternary $In_{1-x}Ga_xAs_yP_{1-y}$ as a well material instead of ternary $In_{1-x}Ga_xAs$. The Ga content x and As content y were adjusted to vary the amount of strain from 1.9% tension of 1.4% compression while maintaining the energy difference between the conduction and valence ground states at 0.95 eV for all quantum wells. The well thickness 6 nm was independent of the amount of strain. The material parameters used in the calculations are listed in Table I. Most of the parameters for $In_{1-x}Ga_xAs_yP_{1-y}$ quaternary compound were derived from the four binary-compound parameters by using an interpolation scheme.[28]

To extract the characteristic features of strain-induced changes in the valence-band structure, we introduced the average effective-mass approximation[26,27] in which the coupled valence bands are approximated by the decou-

TABLE I. Material parameters.

Parameters[a]	GaAs	GaP	InAs	InP
E_g (eV)	1.42	2.74	0.36	1.35
ϵ_s	13.1	11.1	14.6	12.4
ϵ_∞	11.1	8.46	12.25	9.55
ω_{LO} (10^2 cm^{-1})	2.85	4.03	2.39	3.45
m_{el}^*/m_0	0.067	0.17	0.023	0.08
γ_1	6.85	4.05	19.67	4.95
γ_2	2.1	0.49	8.37	1.65
γ_3	2.9	1.25	9.29	2.35
l_a (Å)	5.6533	5.4512	6.0584	5.8688
C_{11} ($\times 10^{11}$ dyn/cm^2)	11.88	14.12	8.329	10.22
C_{12} ($\times 10^{11}$ dyn/cm^2)	5.38	6.253	4.526	5.76
dE_g/dP ($\times 10^{-6}$ eV/bar)	11.5	11.0	10.0	8.5
b (eV)	−1.7	−1.5	−1.8	−2.0

[a]The parameters for binary compounds are taken from Refs. 28 and 29.

pled parabolic bands with averaged effective mass m_n^h. This approximation is schematically explained in Fig. 1, which shows the calculated valence-band structure for tensile-strained, unstrained, and compressive-strained quantum wells. The exact band structure, which was obtained by the $\mathbf{k}\cdot\mathbf{p}$ theory (solid lines), exhibits strong nonparabolicity due to the valence-band mixing. The decoupled parabolic bands (dashed lines) were fitted to each subband of the exact band structure according to the procedure described in Sec. II A. For a given carrier density and the quasi-Fermi level for holes, the effective mass m_n^h of the approximated parabolic band was determined so that the density and the quasi-Fermi level agree with those of the exact band structure. Hence, not only the total carrier density but also the carrier density of each subband is unchanged in this approximation.

Figure 2 shows the variation in the averaged effective mass of the lowest valence subband m_1^h with the amount of strain. The electron effective mass obtained by a linear interpolation is also shown in this figure. In the case of compressive strain, m_1^h decreases monotonically with strain. Applying small amount of tensile strain, m_1^h increases with strain since $|\frac{3}{2},\pm\frac{3}{2}\rangle$ and $|\frac{3}{2},\pm\frac{1}{2}\rangle$ states approach each other, which results in an increase of the density of states due to a strong coupling between these two subbands. Around the critical amount of tensile strain at which they cross over, m_1^h becomes maximum. With the application of larger amount of tensile strain, m_1^h decreases with strain since the coupling between these two states is relaxed. As shown in this figure, the variation of the electron effective mass is less significant throughout the whole range of strain, while the largest hole effective mass is almost five times as large as the smallest one in the range of strain studied. Hence strained $In_{1-x}Ga_xAs_yP_{1-y}$ quaternary compound is an ideal material system to study the direct relationship between the intrasubband scattering rates and the strain-induced changes in the valence-band structures as compared with strained $In_{1-x}Ga_xAs$ ternary compound in which the electron effective mass significantly changes with In content (i.e., the amount of strain).

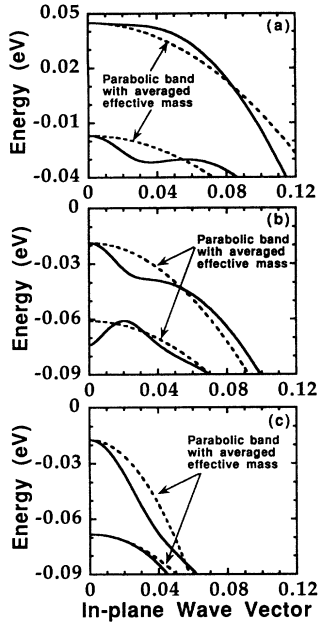

FIG. 1. Valence-band structure of (a) 1.9% tensile-strained, (b) unstrained, and (c) 1.4% compressive-strained $In_{1-x}Ga_xAs_yP_{1-y}$ quantum well. The solid lines are the results calculated by $\mathbf{k}\cdot\mathbf{p}$ theory within the axial approximation and the dashed lines indicate the parabolic bands which are fitted to each valence subband. The well width is 6 nm. Wave vectors are normalized by $2\pi/l_a$, where l_a is a lattice constant of the well. Energies are measured from the top of the valence-band edge for $|\frac{3}{2},\pm\frac{3}{2}\rangle$ states.

B. Intrasubband scattering rates

Figures 3(a) and 3(b) show the hole and electron intrasubband scattering rates plotted as a function of the initial state energy in an unstrained quantum well. The temperature is 300 K and the carrier density (n_s) of each component of the electron-hole plasma is 3×10^{12} cm^{-2}, which is most relevant to the threshold carrier density of QW lasers. The results for three situations are compared: (i) the unscreened phonon system [which uses the dielectric function given in Eq. (11a), dotted line in the figure],

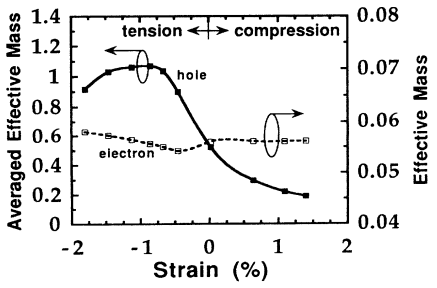

FIG. 2. The averaged effective mass of the lowest valence subband plotted as a function of the amount of strain. The variation of the electron effective mass with the strain is also shown. The effective mass is represented in units of free electron mass m_0.

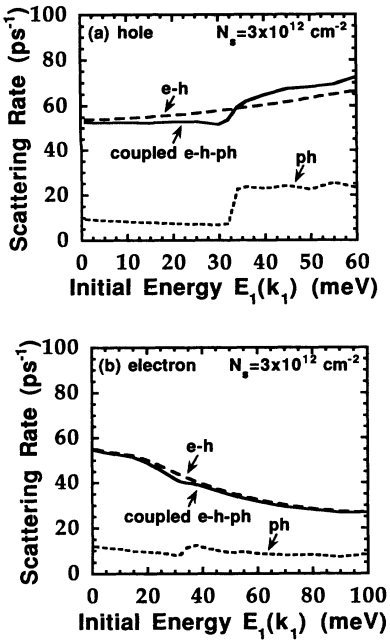

FIG. 3. The intrasubband scattering rates for (a) holes and (b) electrons plotted as a function of the initial state energy $[E_1^\sigma(\mathbf{k}_1)]$ in an unstrained quantum well. The results for three kinds of dielectric functions are compared: *ph* (dotted line), *e-h* (dashed line), and *coupled e-h-ph* (solid line) represent the unscreened phonon system [Eq. (11a)], the screened electron-hole plasma neglecting the phonons [Eq. (11b)], and the screened electron-hole plasma coupled with the phonons [Eq. (11c)], respectively. The quantum-well thickness is 6 nm and the temperature is 300 K unless otherwise specified.

(ii) the screened electron-hole system neglecting the phonons [which uses the dielectric function given in Eq. (11b), dashed line], and (iii) the screened electron-hole system coupled with the phonons [which uses the dielectric function given in Eq. (11c), solid line].

It is interesting to compare the total scattering rate of a carrier in the electron-hole-phonon system by considering the electron-hole plasma coupled and uncoupled with the phonons The latter is the sum of the rates for the cases (i) and (ii), while the former is given by (iii). As can be seen from the results in Fig. 3(a), the scattering rates in the electron-hole plasma uncoupled with the phonons are higher than those in the coupled electron-hole-phonon system. This implies that the hole-phonon interaction is screened by the electron-hole plasma to some extent at this plasma density. Another indication of screening is that the LO-phonon threshold is less pronounced for the coupled electron-hole-phonon system [case (iii)] as compared with that for unscreened phonons [case (i)]. In addition, the hole scattering rates for the electron-hole system [case (ii)] show an almost independent behavior with the initial state energy. Due to the large hole effective mass, the hole distribution function is not degenerate.

For electron scattering, on the other hand, there is no LO-phonon threshold for the coupled electron-hole-phonon system as is shown in Fig. 3(b). This indicates that the electron-phonon interaction is completely screened by the electron-hole plasma at this plasma density. Consequently, the scattering rates obtained by considering the electron-hole plasma without the phonons [case (ii), dashed line] becomes a good approximation as compared to those of the coupled electron-hole-phonon system [case (iii), solid line] as shown in this figure. That the phonons may be neglected for an electron scattering and not for a hole is later explained to result from the electrons' weaker coupling with the phonons, due to the mass dependence of the coupling constant. Another consideration is that since the electron effective mass is much smaller, the electron distribution function becomes degenerate at this plasma density as compared with the holes. This results in the reduction of the scattering rates with initial state energy due to phase-space restrictions.[30] Since Figs. 3(a) and 3(b) demonstrate the importance of a carriers mass on its scattering, it is expected that strain will have a very significant impact on the carriers' mutual interactions.

Before we discuss the mutual interaction in detail, we summarize the important parameters, such as the amount of strain, the plasma frequency, and the Fröhlich coupling constant, to characterize the coupled electron-hole-plasma system. The parameters are shown in Table II. The plasma frequency ($\omega_{\rm pl}$) and the Fröhlich coupling constants for holes ($\alpha_{\rm ph}^h$) and for electrons ($\alpha_{\rm ph}^e$) were calculated by using the following relations:

$$\omega_{\rm pl}^2=\sum_{\sigma,i}\frac{2\pi e^2 q}{\epsilon_\infty}\frac{n_i^\sigma}{m_i^\sigma}\ , \tag{14}$$

$$\alpha_{\rm ph}^\sigma=\left[\frac{1}{\epsilon_\infty}-\frac{1}{\epsilon_s}\right]\frac{e^2}{\hbar}\left[\frac{m_1^\sigma}{2\omega_{\rm LO}}\right]^{1/2}\ . \tag{15}$$

Here e is the free electron charge and $n_i^\sigma(\sigma=e,h)$ is the ith subband carrier density. According to Eq. (14), the plasma frequency can change with the application of strain due to the strain-induced changes in the hole effective mass even if the plasma density is unchanged.

To clarify the mutual interactions between the phonons and the electron-hole plasma, the effects of strain on the scattering rates for both charge carriers were calculated

TABLE II. Strain, LO-phonon frequency, plasma frequency, and Fröhlich coupling constant.

Parameters[a]	Sample I	Sample II	Sample III
Strain (%)	−0.85	no strain	1.4
$\omega_{\rm LO}$ (10^2 cm^{-1})	2.72	2.70	2.88
$\omega_{\rm pl}$[b] (10^2 cm^{-1})	8.26	8.23	8.52
$\omega_{\rm pl}$[c] (10^2 cm^{-1})	2.68	2.66	2.75
$\alpha_{\rm ph}^h$ (hole)	0.298	0.247	0.190
$\alpha_{\rm ph}^e$ (electron)	0.079	0.073	0.089

[a]The plasma frequency ($\omega_{\rm pl}$) and the Fröhlich coupling constants ($\alpha_{\rm ph}^h$ and $\alpha_{\rm ph}^e$) were obtained from Eqs. (14) and (15), respectively.
[b]$\omega_{\rm pl}$ calculated at $n_s=3\times10^{12}$ cm^{-2}.
[c]$\omega_{\rm pl}$ calculated at $n_s=3\times10^{11}$ cm^{-2}.

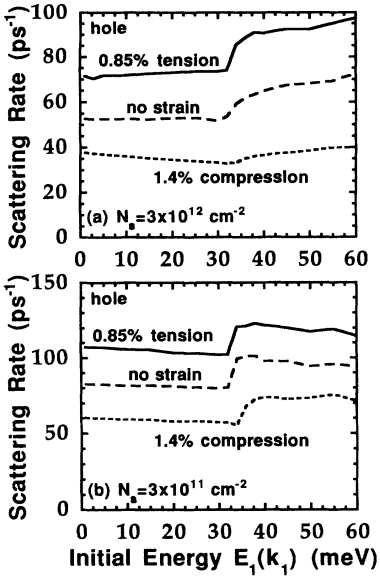

FIG. 4. The hole intrasubband scattering rates for double-component electron-hole plasma density of (a) 3×10^{12} cm^{-2} and (b) 3×10^{11} cm^{-2} plotted as a function of the initial state energy $[E_1^h(\mathbf{k}_1)]$. The solid, dashed, and dotted lines are the results for 0.85% tension, no strain, and 1.4% compression, respectively. The dielectric function for the screened electron-hole plasma with the phonons [Eq. (11c)] is used for the calculations.

for two different plasma densities: 3×10^{12} and 3×10^{11} cm^{-2}. The carrier densities of optically excited or doped semiconductors usually belong to this range. The results for holes are shown in Figs. 4(a) and 4(b). The scattering rates were calculated for three samples with different amount of strain: 0.85% tension (sample I), no strain (sample II), and 1.4% compression (sample III). As shown in Fig. 2, the hole effective mass becomes the largest at the 0.85% tension and the smallest at the 1.4% compression. In Fig. 4(a), for the plasma density of 3×10^{12} cm^{-2}, the LO-phonon threshold becomes more pronounced as the hole effective mass increases. On the other hand, at low densities as shown in Fig. 4(b), the LO-phonon threshold clearly appears regardless of the amount of strain (i.e., the hole effective mass). It is also noted from these results that the larger hole effective mass leads to the larger scattering rates throughout the whole range of the initial-state energy regardless of the plasma density.

The presence and absence of the phonon threshold in Figs. 4(a) and 4(b) are primarily explained by the change in the hole effective mass with strain. For a plasma density of 3×10^{12} cm^{-2}, the plasma frequency ($\omega_{\rm pl}$) is about three times as large as the LO-phonon frequency ($\omega_{\rm LO}$), as shown in Table II. In this situation ($\omega_{\rm LO}<\omega_{\rm pl}$), the electron-hole plasma can respond with higher frequency than the phonons and can follow the motion of the phonons (but not vice versa). Therefore, the screening of the hole-phonon interaction by the high-density electron-hole plasma results in the reduction of the Fröhlich coupling.[3] As shown in Table II, the Fröhlich coupling constant for holes exhibits strain dependence; this is due to the hole mass changing as can be seen from Eq. (15). Hence, due to the small coupling constant in the compressive-strained well ($\alpha_{\rm ph}^h=0.190$), the hole-phonon interaction is more easily screened than in the tensile-strained well ($\alpha_{\rm ph}^h=0.298$). For a plasma density of 3×10^{11} cm^{-2}, the plasma frequency is approximately equal to the LO-phonon frequency ($\omega_{\rm LO}\approx\omega_{\rm pl}$), as shown in Table II. The LO-phonon threshold is clearly observed irrespective of the amount of strain at this density. For this density, the electron-hole screening is sufficiently weak as to be unable to reduce the carrier-phonon interactions. These results indicate that the changes in the hole effective mass due to the application of strain exert a significant influence on the hole scattering rates through corresponding changes in the mutual interactions between the phonons and the electron-hole plasma.

Figures 5(a) and 5(b) are similar to Figs. 4(a) and 4(b), but instead of hole scattering, the electron scattering rates are plotted for the same conditions. The influence of the electron-hole plasma on the electron-phonon interaction is similar to that of holes. At high densities, no LO-phonon threshold is observed in any of the samples, as shown in Fig. 5(a). We recall that the electron effective mass is smaller and shows less strain dependence as compared with holes. Therefore the Fröhlich coupling constants for electrons are much smaller than those for holes and with less strain dependence ($\alpha_{\rm ph}^e=0.073$–0.089). Accordingly, electron-phonon interaction is easily screened by the electron-hole plasma of this density irrespective of the amount of strain and the

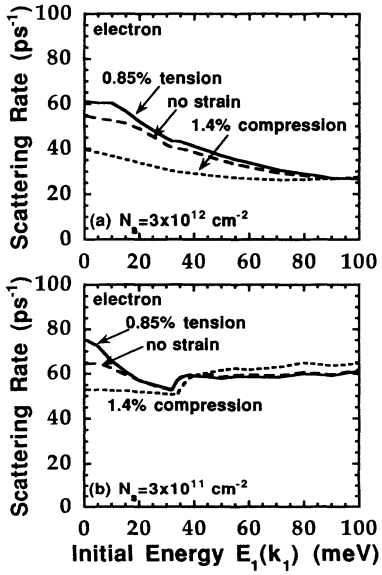

FIG. 5. The electron intrasubband scattering rates for double-component electron-hole plasma density of (a) 3×10^{12} cm^{-2} and (b) 3×10^{11} cm^{-2} plotted as a function of the initial state energy $[E_1^e(\mathbf{k}_1)]$. The solid, dashed, and dotted lines are the results for 0.85% tension, no strain, and 1.4% compression, respectively. The dielectric function for the screened electron-hole plasma with the phonons [Eq. (11c)] is used for the calculations.

LO-phonon threshold disappears in all samples. At low plasma densities, the LO-phonon threshold is clearly observed regardless of the amount of strain as shown in Fig. 5(b). The electron-hole plasma's screening is not strong enough to reduce the electron-phonon interaction. It is also noted that the electron scattering rates near the subband edge increase with the hole mass at both plasma densities. This is attributed to the low and narrow range of energies the holes occupy (due to their larger effective masses), so that low-energy electrons are included to a greater degree than those of high energy.

It is clear from these results that the mutual coupling between the phonons and the electron-hole plasma plays an important role in carrier scattering at the densities most relevant to electronic and optoelectronic device operation, that is, from 3×10^{11} to 3×10^{12} cm^{-2}. The overall results demonstrate that the strain-induced changes in the valence-band structure exert a significant influence on the scattering rates of the electrons as well as the holes.

IV. SUMMARY

We have calculated the intrasubband scattering rates for electrons and holes at finite temperatures in highly excited QW structures with biaxial strain (both compressive and tensile). The characteristic features of the strain-induced changes in the valence-band structures were extracted from the $\mathbf{k}\cdot\mathbf{p}$ results by average effective-mass approximation. Carrier-carrier and carrier-phonon interactions have been taken into account on an equal basis within the fully dynamic random-phase approximation. To properly treat multisubband structures, the effects of carriers occupying higher subbands are consistently included in the RPA dielectric function. The plasma densities considered, 3×10^{11}–3×10^{12} cm^{-2}, are those relevant to electronic and optoelectronic device operation. A discussion of the screening of carrier-phonon interaction by the electron-hole plasma in the coupled electron-hole-phonon system has been presented.

We show that the strain-induced changes exert a pronounced influence on the scattering rates not only for holes but also for electrons. The principal influence of the change in the hole effective mass is the change in the density of final states of the holes and the phonon coupling with holes. The effectiveness of screening at a given carrier density has been shown to depend strongly on the strain-induced changes in the effective mass through changes in the Fröhlich interaction (and of course, carrier density). On the basis of our results, we conclude that the strain-induced changes in the valence-band structure are essential to include in the investigation of carrier scattering in highly excited semiconductor SL QW structures.

ACKNOWLEDGMENTS

The authors would like to thank Karl Hess of University of Illinois for his support and fruitful discussions. S. S. and K. Y. would like to thank Takayuki Yamanaka, Wayne Lui, and Yuzo Yoshikuni for their helpful discussions. They would also like to thank Haruhiko Tsuchiya for his encouragement during the course of this work.

APPENDIX

For the case of strained-layer semiconductor quantum wells in which we are interested, we can assume pseudomorphic epitaxial growth, where the epitaxial semiconductor layer is under biaxial strain. In this case, the strain tensor ϵ_{ij} is represented by

$$\begin{aligned}
&\epsilon_{xx}=\epsilon_{yy}=\frac{l_0-l_a}{l_a}\ ,\\
&\epsilon_{zz}=-\frac{2C_{12}}{C_{11}}\epsilon_{xx}\ ,\\
&\epsilon_{xy}=\epsilon_{yz}=\epsilon_{zx}=0\ ,
\end{aligned}\tag{A1}$$

where l_0 and l_a are the lattice constants of the substrate material and the quantum-well material, respectively, and C_{11} and C_{12} are the stiffness constants.

The Bloch states for holes are expressed as the linear combinations of the products of the spinor and the p-like valence-band Bloch states $|x\rangle$, $|y\rangle$, and $|z\rangle$ and are given by

$$\begin{aligned}
|\psi^h_{3/2}\rangle&=-\frac{1}{\sqrt{2}}(|x\rangle+i|y\rangle)\alpha\ ,\\
|\psi^h_{1/2}\rangle&=-\frac{1}{\sqrt{6}}(|x\rangle+i|y\rangle)\beta+\sqrt{2/3}|z\rangle\alpha\ ,\\
|\psi^h_{-1/2}\rangle&=\frac{1}{\sqrt{6}}(|x\rangle-i|y\rangle)\alpha+\sqrt{2/3}|z\rangle\beta\ ,\\
|\psi^h_{-3/2}\rangle&=\frac{1}{\sqrt{2}}(|x\rangle-i|y\rangle)\beta\ .
\end{aligned}\tag{A2}$$

Here α and β denote the up and down spinors. For this basis set, a 4×4 Luttinger-Kohn Hamiltonian $H_h^{\nu\nu'}$ in Eq. (2) is represented as

$$H_h^{\nu\nu'}=\begin{bmatrix} P+Q & -S & R & 0\\ -S^\dagger & P-Q & 0 & R\\ R^\dagger & 0 & P-Q & S\\ 0 & R^\dagger & S^\dagger & P+Q \end{bmatrix}.\tag{A3}$$

The matrix elements of $H_h^{\nu\nu'}$ are given by

$$\begin{aligned}
P&=P_k+P_\epsilon\ ,\\
Q&=Q_k+Q_\epsilon\ ,\\
P_k&=\frac{\hbar^2}{2m_0}\gamma_1(k_x^2+k_y^2+k_z^2)\ ,\\
Q_k&=\frac{\hbar^2}{2m_0}\gamma_2(k_x^2+k_y^2-2k_z^2)\ ,\\
S&=\frac{\hbar^2}{2m_0}2\sqrt{3}\gamma_3(k_x-ik_y)k_z\ ,\\
R&=-\frac{\hbar^2}{2m_0}2\sqrt{3}[\gamma_2(k_x^2-k_y^2)-2i\gamma_3k_xk_y]\ ,\\
P_\epsilon&=-a_v(\epsilon_{xx}+\epsilon_{yy}+\epsilon_{zz})\ ,\\
Q_\epsilon&=-\frac{b}{2}(\epsilon_{xx}+\epsilon_{yy}-2\epsilon_{zz})\ ,
\end{aligned}\tag{A4}$$

where γ_1, γ_2, and γ_3 are Luttinger parameters, m_0 is the free electron mass, i is the pure imaginary, a_v is the hydrostatic deformation potential for the valence band, and b is the shear deformation potential.

The conduction-band Hamiltonian H_e in Eq. (3) is given by

$$H_e=\frac{\hbar}{2m_e(z)}(k_x^2+k_y^2+k_z^2)+a_c(\epsilon_{xx}+\epsilon_{yy}+\epsilon_{zz}) , \quad \text{(A5)}$$

where $m_e(z)$ is the electron effective mass and a_c is the hydrostatic deformation potential for the conduction band. The total hydrostatic deformation potential $a=a_c+a_v$ is given by

$$a=-\frac{(C_{11}+2C_{12})}{3}\frac{dE_g}{dP} . \quad \text{(A6)}$$

Here dE_g/dP is the hydrostatic pressure dependence of energy band gap.[31]

[1]H. Haug and S. Schmitt-Rink, Prog. Quantum Electron. **9**, 3 (1984).

[2]G. D. Mahan, *Many-Particle Physics,* 2nd ed. (Plenum, New York, 1986); see also D. Pines and P. Nozieres, *The Theory of Quantum Liquids* (Addison-Wesley, New York, 1989); B. K. Ridley, *Quantum Processes in Semiconductors,* 2nd ed. (Oxford, New York, 1988).

[3]R. Zimmermann, *Many-Particle Theory of Highly Excited Semiconductors* (Teubner, Leipzig, 1988).

[4]R. Binder, D. Scott, A. E. Paul, M. Lindberg, K. Henneberger, and S. W. Koch, Phys. Rev. B **45**, 1107 (1992).

[5]M. Asada, IEEE J. Quantum Electron. **QE-25**, 2019 (1989).

[6]W. Xiaoguang, F. M. Peeters, and J. T. Devreese, Phys. Rev. B **32**, 6982 (1985).

[7]R. Jalabert and S. Das Sarma, Phys. Rev. B **40**, 9723 (1989).

[8]S. K. Lyo, Phys. Rev. B **43**, 7091 (1991).

[9]H. Haug and S. W. Koch, *Quantum Theory of the Optical and Electronic Properties of Semiconductors,* 2nd ed. (World Scientific, Singapore, 1993).

[10]S. W. Kirchoefer, N. Holonyak, Jr., K. Hess, K. Meehan, D. A. Gulino, H. G. Drickamer, J. J. Coleman, and P. D. Dapkus, J. Appl. Phys. **53**, 6037 (1982).

[11]G. C. Osbourn, Phys. Rev. B **27**, 5126 (1983).

[12]E. Yablonovitch and E. O. Kane, IEEE J. Lightwave Technol. **LT-4**, 504 (1986).

[13]A. R. Adams, Electron. Lett. **22**, 249 (1986).

[14]P. J. A. Thijs, L. F. Tiemeijer, P. I. Kuindersma, J. J. M. Binsma, and T. van Dongen, IEEE J. Quantum Electron. **QE-27**, 1426 (1991).

[15]E. P. O'Reilly, Semicond. Sci. Technol. **4**, 121 (1989).

[16]H. Haug and S. W. Koch, Phys. Rev. A **39**, 1887 (1989).

[17]W. H. Knox, D. S. Chemla, G. Livescu, J. E. Cunningham, and J. E. Henry, Phys. Rev. Lett. **61**, 1290 (1988).

[18]J. A. Kash, Phys. Rev. B **40**, 3455 (1989).

[19]P. Sotirelis, P. von Allmen, and K. Hess, Phys. Rev. B **47**, 12 744 (1993).

[20]S. L. Chuang, Phys. Rev. B **43**, 9649 (1991).

[21]S. Seki, P. Sotirelis, K. Hess, T. Yamanaka, and K. Yokoyama, Appl. Phys. Lett. **61**, 2147 (1992).

[22]J. M. Luttinger and W. Kohn, Phys. Rev. **97**, 869 (1955).

[23]G. Bastard, *Wave Mechanics of Semiconductor Heterostructures* (Les Editions de Physique, Paris, 1989).

[24]D. A. Broido and L. J. Sham, Phys. Rev. B **31**, 888 (1985).

[25]A. Twardowski and C. Hermann, Phys. Rev. B **35**, 8144 (1987).

[26]S. Seki and K. Yokoyama, J. Appl. Phys. **74**, 4242 (1993).

[27]M. F. Pereira, Jr. and S. W. Koch, J. Opt. Soc. Am. B **10**, 765 (1993).

[28]S. Adachi, J. Appl. Phys. **53**, 8775 (1982).

[29]L. Landolt-Börnstein, *Numerical Data and Functionships in Science and Technology,* edited by O. Madelung (Springer, Berlin, 1982), Vol. 17a; *ibid.* (1986), Vol. 22a.

[30]H. Haug and D. B. Tran Thoai, Phys. Status Solidi B **98**, 581 (1980).

[31]G. Ji, D. Huang, U. K. Reddy, T. S. Henderson, R. Houdré, and H. Morkoç, J. Appl. Phys. **62**, 3366 (1987).